metals

MDPI

Article

Phase Diagram of near Equiatomic Zr-Pd Alloy

Mitsuhiro Matsuda [1,*], Tomohiro Nishiura [2,†], Takateru Yamamuro [3] and Minoru Nishida [4]

1 Division of Materials Science, Faculty of Advanced Science and Technology, Kumamoto University, Kumamoto 860-8555, Japan
2 Interdisciplinary Graduate School of Science and Engineering, Kyushu University, Kasuga, Fukuoka 816-8580, Japan; nishiura.2yh.tomohiro@jp.nssmc.com
3 Technical Division, Faculty of Engineering, Kumamoto University, Kumamoto 860-8555, Japan; yamamuro@tech.eng.kumamoto-u.ac.jp
4 Department of Advanced Materials Science and Engineering, Faculty of Engineering Sciences, Kyushu University, Kasuga, Fukuoka 816-8580, Japan; nishida.minoru.355@m.kyushu-u.ac.jp
* Correspondence: matsuda@alpha.msre.kumamoto-u.ac.jp; Tel.: +81-96-342-3718
† Present address: Advanced Technology Research Laboratories, Nippon Steel & Sumitomo Metal Corporation, 1-8 Fuso-Cho, Amagasaki, Hyogo 660-0891, Japan.

Received: 28 April 2018; Accepted: 18 May 2018; Published: 21 May 2018

Abstract: The exact eutectoid and peritectoid temperatures in near equiatomic Zr-Pd compositions have been determined by using the diffusion couple method and microstructure analysis. The crystal structure of $Zr_{13}Pd_{12}$ compound were estimated to be orthorhombic with a = 1.78 nm, b = 0.80 nm and c = 1.00 nm from the electron diffraction experiments. The $Zr_{13}Pd_{12}$ compound is formed at 1100 ± 2 K with a peritectoid reaction between Zr_2Pd and ZrPd compounds. The ZrPd compound transforms to $Zr_{13}Pd_{12}$ and Zr_9Pd_{11} compounds by a eutectoid reaction at 1028 ± 4 K. Based on these results, the phase diagram of near equiatomic Zr-Pd binary system is reconstructed.

Keywords: Zr-Pd alloy; crystal structure; microstructure; phase diagrams; transmission electron microscopy

1. Introduction

Recently, the interest in shape memory alloys with high transformation temperatures (HTSMAs), defined as SMAs that operate at temperature above 373 K, has significantly increased [1–3]. Near equiatomic Zr-Pd alloys are candidates for HTSMAs because of high martensitic transformation temperature; they undergo a martensitic transformation from a cubic B2-type parent phase to an orthorhombic CrB-type martensitic phase at 813 K, and monoclinic martensitic phase at room temperature [4]. In order to develop the new HTSMAs, correct information on transformation behavior and phase equilibrium is inevitably required. Phase diagrams, which are composed of lines of the equilibrium and phase boundaries, are useful for not only the development of new alloys for specific applications, but also design and control of heat-treatment procedures to supply a desired mechanical, functional, and chemical property. Therefore, Zr-Pd binary phase diagrams, based on the experimental data [5] and by the CALPHAD technique using a computational optimization procedure [6], have been reported. Also, one of the authors has proposed a modified Zr-Pd phase diagram by using solution-treated and aged specimens with various compositions and diffusion couples, as follows [7]. The ZrPd compound transforms to $Zr_{13}Pd_{12}$ and Zr_9Pd_{11} compounds by a eutectoid reaction at about 1040 K. It is also found that the $Zr_{13}Pd_{12}$ compound forms by a peritectoid reaction between Zr_2Pd and ZrPd compounds at about 1100 K. However, the exact eutectoid and peritectoic temperatures are not determined. In addition, the crystal structure of newly discovered $Zr_{13}Pd_{12}$ compound is not analyzed.

It is aim of the present paper is to determine the exact eutectoid and peritectoid temperatures by using the diffusion couple method and microstructure analysis. Crystal structure and the lattice parameters of the $Zr_{13}Pd_{12}$ compound is also estimated from the electron diffraction experiments. Based on these results, the phase diagram of near equiatomic Zr-Pd binary system is reconstructed.

2. Materials and Methods

Zr-15 to 60 atom % Pd alloys were prepared from 99.7% Zr and 99.97% Pd (mass %) by arc melting in an argon atmosphere. The ingots were homogenized at 1273 K for 36 ks in vacuum. Disks with a diameter of 3 mm were spark-cut from the ingot for the transmission electron microscope (TEM) (JEOL, Tokyo, Japan) studies. They were solution-treated in vacuum at 1273 K for 3.6 ks, and then quenched in ice water. Some of specimens were aged from 973 to 1273 K for 3.6–720 ks. Diffusion couples with combination of Zr-15 atom % Pd/Zr-60 atom % Pd alloys were prepared by a partial arc melting. Diffusion couples were annealed at 1023 K and 1033 K for 720 ks, and then quenched into ice water. Concentration–penetration profiles in the diffusion zone were obtained by electron probe microanalysis, using a JXA-8900 microscope (JEOL, Tokyo, Japan). Microstructure examination of some alloys after heat treatment was carried out by scanning electron microscope (SEM), using a JSM-5600LV microscope (JEOL, Tokyo, Japan). The solution-treated disks with a diameter of 3 mm were ground to at thickness of 90 μm. They were dimpled with a GATAN Model 656 and Ar-ion milled with a GATAN Model 691 PIPS (GATAN, Pleasanton, CA, USA). TEM was also applied to the identification of crystal structure and defects in various phases after heat treatment, using a JEM-2000FX microscope with an accelerating voltage of 200 kV. The selected area diffraction patterns were taken using the aperture with a physical diameter of 10 μm corresponding to an optical diameter in the image plane of about 150 nm. The following lattice parameters were used for the analysis of the monoclinic ZrPd martensite: a_{ZrPd} = 0.666 nm, b_{ZrPd} = 0.875 nm, and c_{ZrPd} = 0.542 nm [4], and the tetragonal Zr_9Pd_{11} compound: $a_{Zr_9Pd_{11}}$ = 1.031 nm and $c_{Zr_9Pd_{11}}$ = 0.694 nm [5], and the tetragonal Zr_2Pd compound: a_{Zr_2Pd} = 0.331 nm and c_{Zr_2Pd} = 1.089 nm [8], respectively.

3. Results and Discussion

Figure 1a,b show the Zr-Pd binary phase diagrams evaluated by data from [5] and the summary of all the present experimental results plotted between Zr_2Pd and Zr_3Pd_4 compounds, respectively. Especially, the phase diagram of near equiatomic Zr-Pd composition is reconstructed. Major modifications are summarized as follows. $Zr_{13}Pd_{12}$ compound has an orthorhombic structure, and its lattice parameters were estimated to be a = 1.78 nm, b = 0.80 nm and c = 1.00 nm from the electron diffraction experiments. The $Zr_{13}Pd_{12}$ compound is formed at 1100 ± 2 K with a peritectoid reaction between Zr_2Pd and ZrPd compounds in Zr-48.0 atom % Pd. The ZrPd compound transforms to $Zr_{13}Pd_{12}$ and Zr_9Pd_{11} compounds by a eutectoid reaction at 1028 ± 4 K in Zr-49.5 atom % Pd ± 0.4 atom % Pd composition. The evidence of these modifications is discussed below.

3.1. Microstructural Analysis of $Zr_{13}Pd_{12}$ Compound by the Electron Diffraction Experiments

Figure 2a shows a typical bright field image of the Zr-49 atom % Pd alloy aged at 1073 K for 720 ks. The electron diffraction patterns in Figure 2b,c are taken from the areas marked B and C in Figure 2a, respectively. The pattern shown in Figure 2b consists of two sets of reflections, which are in mirror symmetry with respect to the $(111)_{ZrPd}$ plane, from the $[\bar{3}12]_{ZrPd}$ direction of the monoclinic ZrPd martensite [4]. The trace of boundaries in region B is parallel to the $(111)_{ZrPd}$ plane. This fact indicates that the two sets of reflections show a $(111)_{ZrPd}$ twin. These observations are consistent with the results reported previously [4,7]. The pattern shown in Figure 2c can be indexed according to the orthorhombic $Zr_{13}Pd_{12}$ compound, as described below.

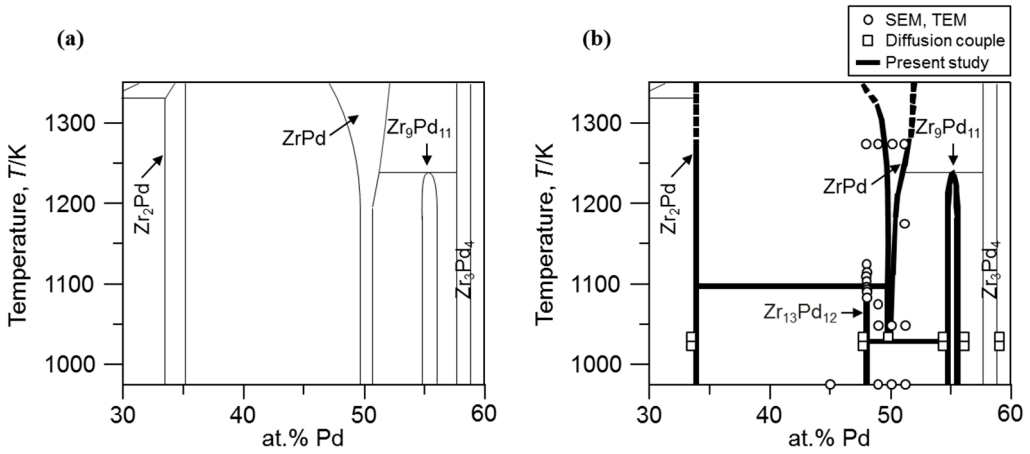

Figure 1. (**a**,**b**) shows the Zr-Pd binary phase diagrams evaluated by data from [5] and the summary of all the present experimental results plotted between Zr_2Pd and Zr_3Pd_4 compounds, respectively. Open circles indicate SEM and TEM observation, and squares are obtained from the diffusion couple experiments.

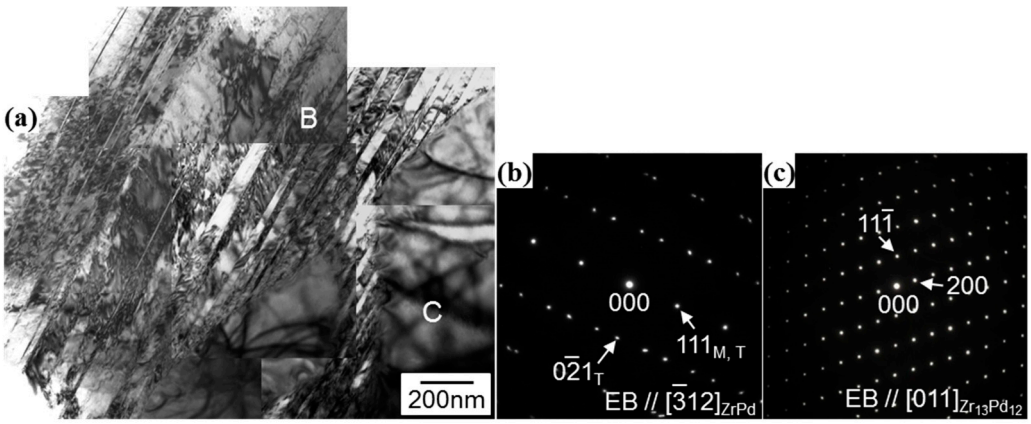

Figure 2. Bright field image in the Zr-49 atom % Pd alloy aged at 1073 K for 720 ks. (**b**,**c**) Electron diffraction patterns taken from the areas marked B and C in (**a**), respectively. The pattern shown in (**b**) consists of two sets of reflections, showing a $(111)_{ZrPd}$ twin pattern, and the platelet is a $(111)_{ZrPd}$ twin. The pattern shown in (**c**) is indexed according to the orthorhombic $Zr_{13}Pd_{12}$ compound.

In order to determine exactly the crystal structure of $Zr_{13}Pd_{12}$ compound, diffraction patterns were taken from a single phase of $Zr_{13}Pd_{12}$ compound by tilting a TEM specimen in the Zr-48 atom % Pd alloy aged at 1083 K for 720 ks. As a clue to analyze those patterns, we refer to the $Ni_{13}Sn_{12}$ compound with orthorhombic system in Ni–Sn alloy [9], because $Ni_{13}Sn_{12}$ compound has the same atomic ratio of composition as $Zr_{13}Pd_{12}$ compound. We therefore assume that Figure 3a is the electron diffraction pattern taken along the [100] direction of the $Zr_{13}Pd_{12}$ compound. On the basis of this hypothesis, the spot distribution on either side of the c^*-axis is symmetric, and the c^*-axis is perpendicular to the b^*-axis, as seen from the dotted lines in Figure 3a–d, which show the electron diffraction patterns obtained by tilting some areas around the c^*-axis of the $Zr_{13}Pd_{12}$ compound. As shown in Figure 3d, the spot distribution on either side of the c^*-axis is symmetric, and the c^*-axis is perpendicular to the a^*-axis. It should be noted that the intensity of the 00l reflections for odd l disappears on tilting around the c^*-axis from the [110] zone axis, as indicated by the arrows in Figure 3c, provided that no 00l reflection for odd l exist in Figure 3c. The 00l reflections in Figure 3a,b are considered to be due to multiple diffraction. The space group satisfying with these extinction rules is $Cmc2_1$, $C2cm$, and $Cmcm$. However, only extinction rules considering even Figure 3e,f cannot determine one of those three space

groups of $Zr_{13}Pd_{12}$ compound. Convergent-beam electron diffraction analysis or high-angle annular dark field scanning transmission electron microscopy observations should be performed to identify it. At least, its lattice parameters can be estimated to be a = 1.78 nm, b = 0.80 nm, and c = 1.00 nm from the present electron diffraction experiments.

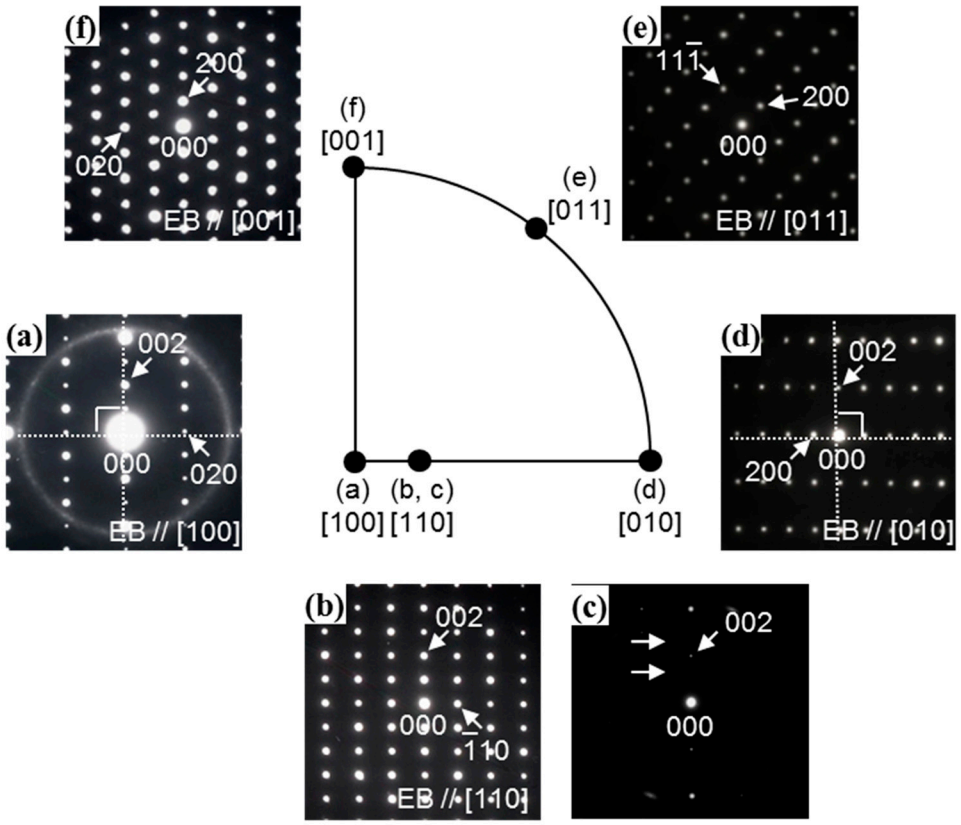

Figure 3. Electron diffraction patterns from the principal zone axes in a single phase of $Zr_{13}Pd_{12}$ compound in the Zr-48 atom % Pd alloy aged at 1083 K for 720 ks, providing the space group: *Cmc*2_1, *C*2*cm*, and *Cmcm* by extinction rules. (**a**) [100]; (**b**) [110]; (**c**) The observed pattern tilting around the c^*-axis from the [110] zone axis; (**d**) [010]; (**e**) [011]; (**f**) [001] zone axes.

3.2. Determination of Eutectoid and Peritectoid Temperatures

Figure 4a–c show the SEM images of Zr-49, 50, and 51 atom % Pd alloys aged at 1273 K for 3.6 ks, respectively. Zr-49 atom % Pd alloy consists of both the monoclinic ZrPd martensitic phase, showing the surface relief, and Zr_2Pd phase, as shown in Figure 4a. On the other hand, both Zr-50 and 51 atom % Pd alloys are composed of only monoclinic Zr-Pd martensitic phase, as shown in Figure 4b,c, respectively. These are consistent with the results of TEM observations, although the micrographs are not included here. Figure 4d–f show the SEM images of Zr-49, 50, and 51 atom % Pd alloys aged at 1048 K for 90 ks, respectively. Based on the TEM analysis in Figure 2, Zr-49 atom % Pd alloy is composed of the $Zr_{13}Pd_{12}$ precipitate in the ZrPd martensitic matrix, as shown in Figure 4d. Zr-50 and 51 atom % Pd alloy consist of two phases, as shown in Figure 4e,f, respectively. In order to identify those phases, TEM observation was performed. Figure 5 shows a typical bright field image in the Zr-51 atom % Pd alloy aged at 1173 K for 720 ks. The electron diffraction patterns in Figure 5b,c are taken from the areas marked B and C in Figure 5a, respectively. The pattern shown in Figure 5b shows a $(1\bar{1}1)_{ZrPd}$ twin pattern of ZrPd martensitic phase, as well as Figure 2. The pattern shown in Figure 5c is indexed according to the Zr_9Pd_{11} compound. Therefore, Figure 4e,f show the Zr_9Pd_{11} precipitates in ZrPd martensitic matrix, indicating that the region of single phase of ZrPd compound narrows with a decrease in temperature.

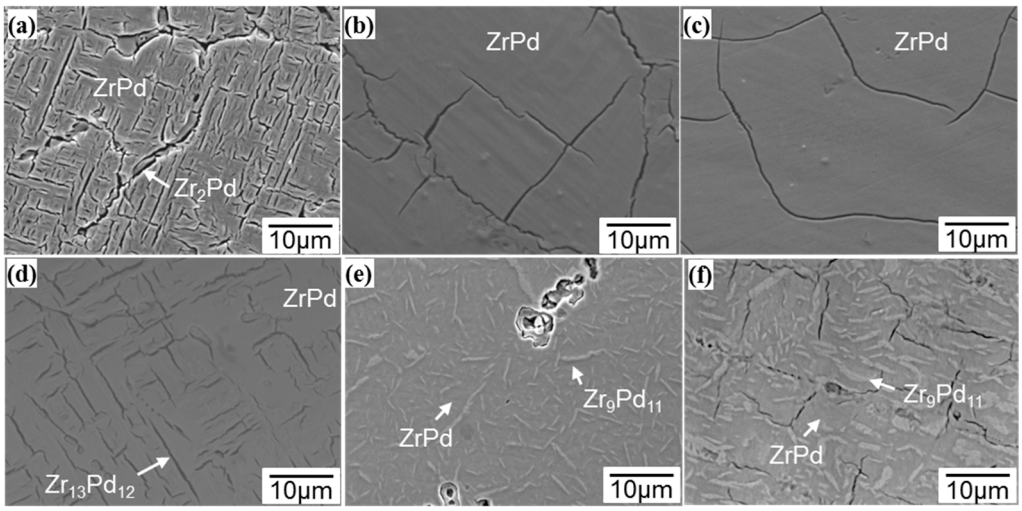

Figure 4. (**a**–**c**) SEM images of Zr-49, 50, and 51 atom % Pd alloys aged at 1273 K for 3.6 ks, respectively. Zr-49 atom % Pd alloy consist of both the monoclinic ZrPd martensitic phase showing the surface relief and Zr_2Pd phase, as shown in (**a**). On the other hand, each Zr-50 and 51 atom % Pd alloy is composed of only ZrPd martensitic phase, as shown in (**b**,**c**), respectively. (**d**–**f**) SEM images of Zr-49, 50, and 51 atom % Pd alloys aged at 1048 K for 90 ks, respectively. Zr-49 atom % Pd alloy is composed of the $Zr_{13}Pd_{12}$ precipitate in the ZrPd martensitic matrix, as shown in (**d**). Zr-50 and 51 atom % Pd alloy consist of two phases, that is, the Zr_9Pd_{11} precipitates in ZrPd martensitic matrix, as shown in (**e**,**f**), respectively.

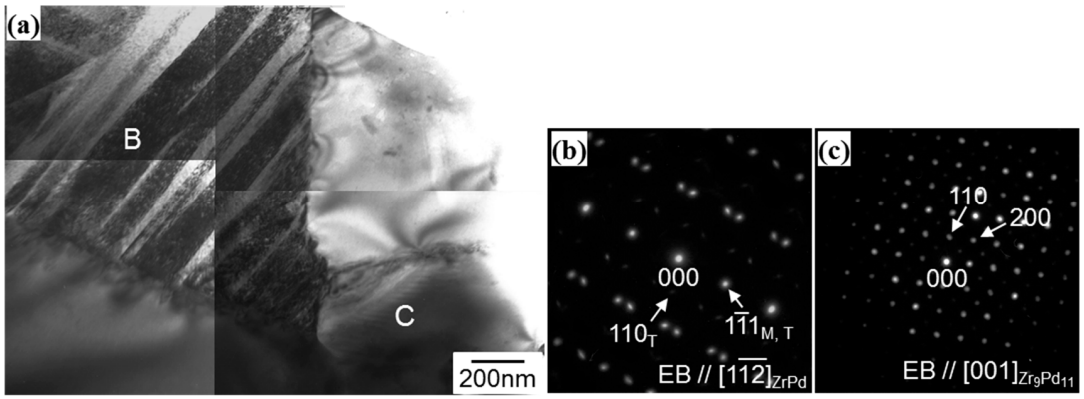

Figure 5. (**a**) Bright field image of the Zr-51 atom % Pd alloy aged at 1173 K for 720 ks. (**b**,**c**) Electron diffraction patterns taken from the areas marked B and C in (**a**), respectively. The pattern shown in (**b**) shows a $(1\bar{1}1)_{ZrPd}$ twin pattern of ZrPd martensitic phase as well as Figure 2. The pattern shown in (**c**) is indexed according to the Zr_9Pd_{11} compound.

Figure 6a–c show the SEM images of Zr-49, 50, and 51 atom % Pd alloys aged at 973 K for 3.6 ks. All the specimens consist of the two phases. In order to identify those phases, TEM observation was performed. Figure 7 shows a typical bright field image in the Zr-51 atom % Pd alloy aged at 973 K for 720 ks. The electron diffraction patterns in Figure 7b,c are taken from the areas marked B and C in Figure 7a, respectively. The patterns shown in Figure 7b,c are indexed according to the $Zr_{13}Pd_{12}$ and Zr_9Pd_{11} compounds, respectively. On the basis of these TEM analyses, two phases in each Figure 6a–c are identified as the $Zr_{13}Pd_{12}$ and Zr_9Pd_{11} compounds, respectively.

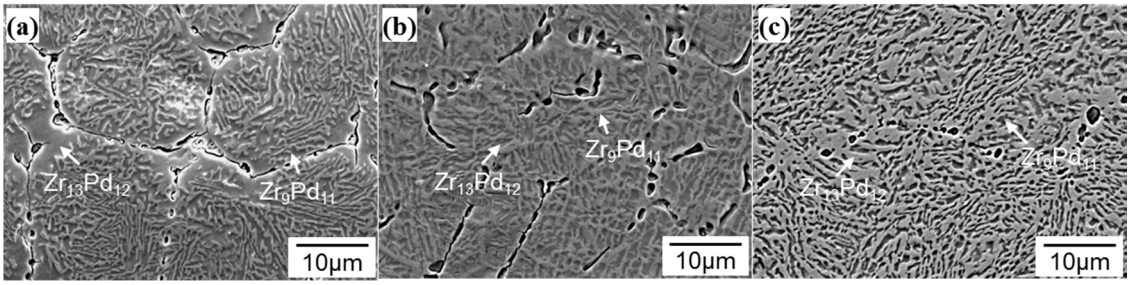

Figure 6. (**a**–**c**) SEM images of Zr-49, 50, and 51 atom % Pd alloys aged at 973 K for 3.6 ks, respectively. All the specimens consist of the $Zr_{13}Pd_{12}$ and Zr_9Pd_{11} compounds.

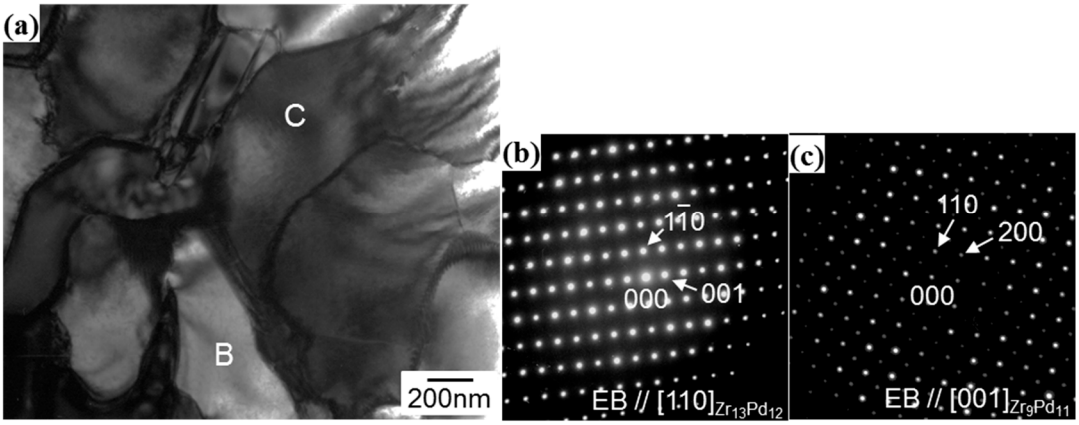

Figure 7. (**a**) Bright field image of the Zr-51 atom % Pd alloy aged at 973 K for 720 ks. (**b**,**c**) Electron diffraction patterns are taken from the areas marked B and C in (**a**), respectively. The patterns shown in (**b**,**c**) are indexed according to the $Zr_{13}Pd_{12}$ and Zr_9Pd_{11} compounds, respectively.

In order to determine the eutectoid temperature, diffusion couple experiments have been carried out. Figure 8a,b shows the SEM image and the corresponding concentration–penetration curves by electron probe microanalysis in the vicinity of the diffusion zone in Zr-15 atom % Pd/Zr-60 atom % Pd couple annealed at 1033 K for 3600 ks, respectively. We can recognize five regions by the difference of image contrasts in Figure 8a, and the four concentration gaps corresponding to $Zr_2Pd/Zr_{13}Pd_{12}$, $Zr_{13}Pd_{12}/ZrPd$, $ZrPd/Zr_9Pd_{11}$, and Zr_9Pd_{11}/Zr_3Pd_4 boundaries by the intensity ratio of Zr and Pd in Figure 8b. Figure 8c,d show the SEM images and the corresponding concentration–penetration curve by electron probe microanalysis in the vicinity of the diffusion zone in Zr-15 atom % Pd/Zr-60 atom % Pd couple annealed at 1023 K for 3600 ks. There are four regions and the three concentration gaps corresponding to $Zr_2Pd/Zr_{13}Pd_{12}$, $Zr_{13}Pd_{12}/Zr_9Pd_{11}$, and Zr_9Pd_{11}/Zr_3Pd_4 boundaries. Compared with these results, ZrPd compound exists in the specimen aged at 1033 K, as shown in Figure 8a.b, but there is no ZrPd compound in the specimen aged at 1023 K, as shown in Figure 8c,d. Consequently, the temperature of eutectoid reaction is estimated to be 1028 $\pm$ 4 K. In order to verify the eutectoid reaction, TEM observation was also performed in Zr-45 atom % Pd alloy. Figure 9a–c show the bright field image and corresponding diffraction pattern in Zr-45 atom % Pd alloy aged at 973 K for 720 ks, respectively. We can index those phases as $Zr_{13}Pd_{12}$ and Zr_2Pd compounds, indicating validity of the suggesting phase diagram of Figure 1.

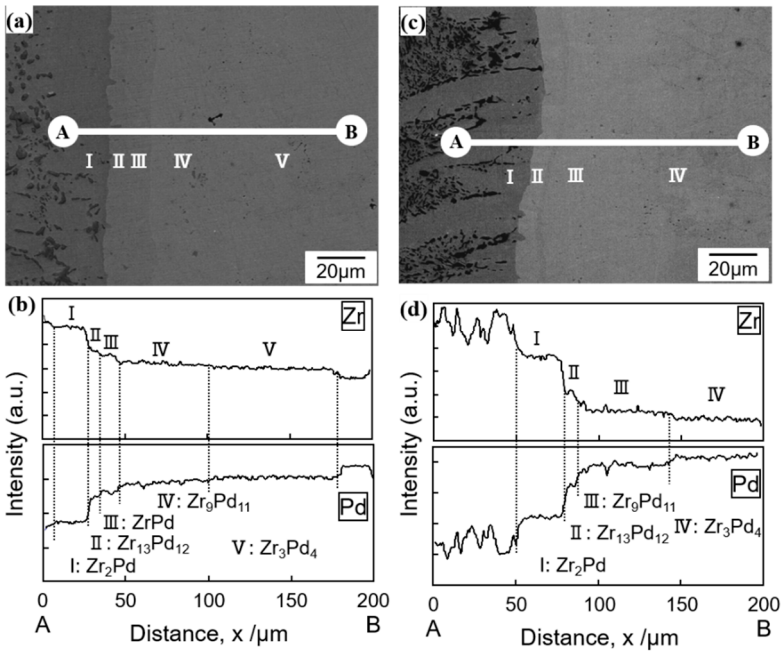

Figure 8. (**a**,**b**) SEM image and the corresponding concentration–penetration curves by electron probe microanalysis in the vicinity of the diffusion zone in Zr-15 atom % Pd/Zr-60 atom % Pd couple annealed at 1033 K for 3600 ks, respectively. There are four concentration gaps corresponding to $Zr_2Pd/Zr_{13}Pd_{12}$, $Zr_{13}Pd_{12}/ZrPd$, $ZrPd/Zr_9Pd_{11}$, and Zr_9Pd_{11}/Zr_3Pd_4 boundaries by the intensity ration of Zr and Pd; (**c**,**d**) SEM image and the corresponding concentration–penetration curves by electron probe microanalysis in the vicinity of the diffusion zone in Zr-15 atom % Pd/Zr-60 atom % Pd couple annealed at 1023 K for 3600 ks. There are three concentration gaps corresponding to $Zr_2Pd/Zr_{13}Pd_{12}$, $Zr_{13}Pd_{12}/Zr_9Pd_{11}$, and Zr_9Pd_{11}/Zr_3Pd_4 boundaries. ZrPd compound exists in the specimen aged at 1033 K, as shown in (**a**,**b**), but there is no ZrPd compound in the specimen aged at 1023 K, as shown in (**c**,**d**).

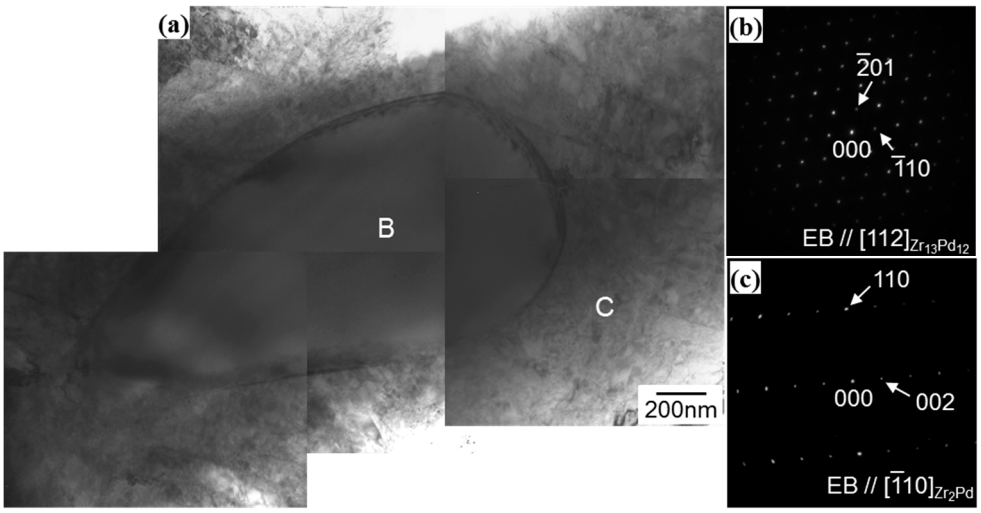

Figure 9. (**a**) Bright field image and (**b**,**c**) corresponding diffraction pattern of Zr-45 atom % Pd alloy aged at 973 K for 720 ks. We can index those phases as $Zr_{13}Pd_{12}$ and Zr_2Pd compounds, respectively.

In order to determine the peritectoid temperature, Zr-48.0 atom % Pd alloy quenched from 1273 K, and aged at 1083 to 1123 K for 720 ks. Specimens aged above 1103 K shown in Figure 10a–e consist of ZrPd and Zr_2Pd phase. On the other hand, those aged below 1098 K shown in Figure 10f–i are

composed of three phases, indicating that $Zr_{13}Pd_{12}$ compound is formed by a peritectoid reaction between Zr_2Pd and ZrPd phases. TEM observations were performed to confirm this peritectoid reaction. Figure 11a shows the bright field image of Zr-48 atom % Pd alloy aged at 1098 K for 720 ks. Electron diffraction patterns in Figure 11b–d are taken from the areas marked B, C, and D in a, respectively. These patterns can be indexed consistently with ZrPd, $Zr_{13}Pd_{12}$, and Zr_2Pd phases, respectively. Based on the SEM images of Figure 10 and TEM analysis of Figure 11, $Zr_{13}Pd_{12}$ compound is also clearly seen at the boundary between Zr_2Pd and ZrPd compounds. Consequently, it is concluded that the $Zr_{13}Pd_{12}$ compound is formed at 1100 ± 2 K with peritectoid reaction between Zr_2Pd and ZrPd compounds in Zr-48.0 atom % Pd.

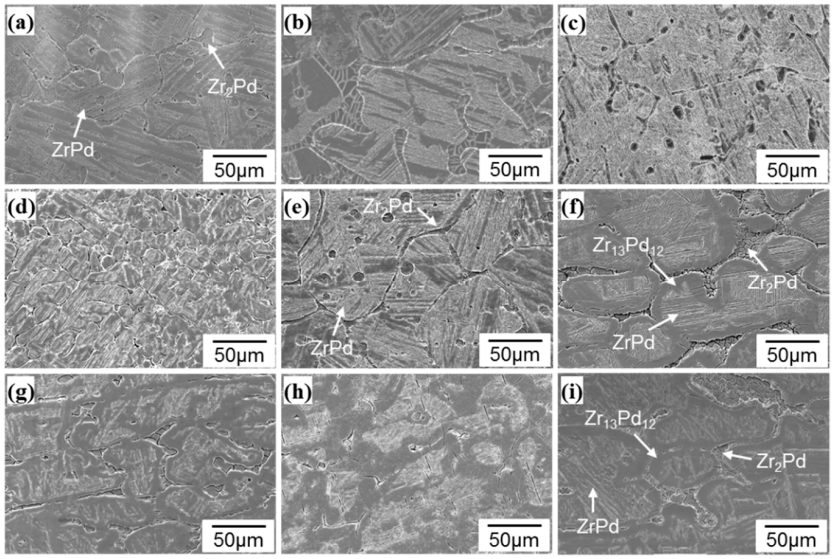

Figure 10. SEM images of Zr-48.0 atom % Pd alloy: (**a**) solution treated and quenched from 1273 K; aged at each temperature for 720 ks; (**b**) 1123 K; (**c**) 1113 K; (**d**) 1108 K; (**e**) 1103 K; (**f**) 1098 K; (**g**) 1093 K; (**h**) 1088 K; and (**i**) 1083 K, respectively.

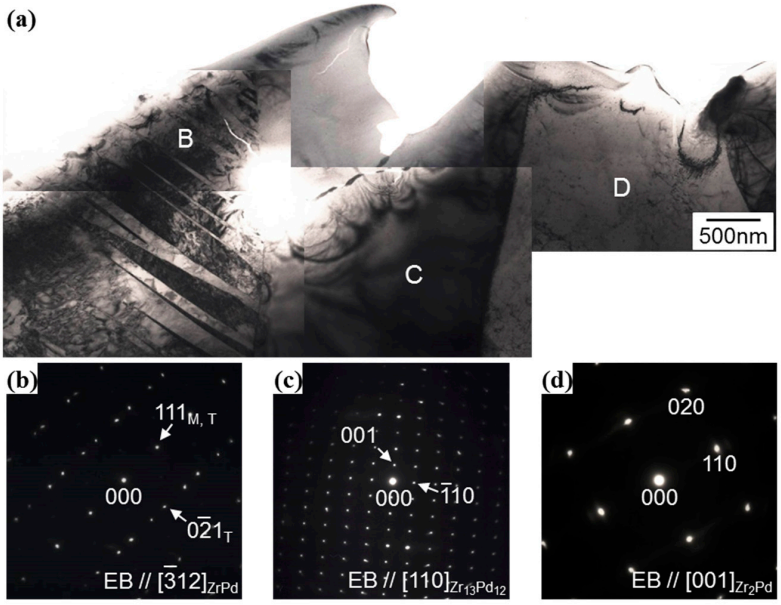

Figure 11. (**a**) Bright field image of Zr-48.0 atom % Pd alloy aged at 1098 K for 720 ks. (**b**–**d**) Electron diffraction patterns taken from the areas marked B, C, and D in (**a**), respectively. These patterns can be indexed consistently with ZrPd, $Zr_{13}Pd_{12}$, and Zr_2Pd phases, respectively.

4. Conclusions

The exact eutectoid and peritectoid temperatures in near equiatomic Zr-Pd compositions have been determined by using the diffusion couple method and microstructure analysis. The crystal structure of $Zr_{13}Pd_{12}$ compound was estimated to be orthorhombic with a = 1.78 nm, b = 0.80 nm, and c = 1.00 nm from the electron diffraction experiments, providing the space group: $Cmc2_1$, $C2cm$, and $Cmcm$ by the extinction rules. The $Zr_{13}Pd_{12}$ compound is formed at 1100 $\pm$ 2 K with a peritectoid reaction between Zr_2Pd and ZrPd compounds. The ZrPd compound transforms to $Zr_{13}Pd_{12}$ and Zr_9Pd_{11} compounds by a eutectoid reaction at 1028 $\pm$ 4 K. Based on these results, the phase diagram of a near equiatomic Zr-Pd binary system is reconstructed.

Author Contributions: M.M. and M.N. wrote the manuscript. All of the authors contributed to the results and results and reviewed the manuscript.

Funding: This research received no external funding.

Conflicts of Interest: The authors declare no conflict of interest.

References

1. Ma, J.; Karaman, I.; Noebe, R.D. High temperature shape memory alloys. *Int. Mater. Rev.* **2010**, *55*, 257–315. [CrossRef]
2. Humbeeck, J.V. Shape memory alloys with high transformation temperatures. *Mater. Res. Bull.* **2012**, *47*, 2966–2968. [CrossRef]
3. Jani, J.M.; Leary, M.; Subic, A.; Gibson, M.A. A review of shape memory alloy research, applications and opportunities. *Mater. Des.* **2014**, *56*, 1078–1113. [CrossRef]
4. Bendersky, L.A.; Stalick, J.K.; Portier, R.; Waterstrat, R.M. Crystallogrphic structures and phase transformations in ZrPd. *J. Alloys Compd.* **1996**, *236*, 19–25. [CrossRef]
5. Waterstrat, R.M.; Shapiro, A.; Jeremie, A. The palladium-zirconium phase diagram. *J. Alloys Compd.* **1999**, *290*, 63–70. [CrossRef]
6. Cuiping, G.; Zhenmin, D.; Changrong, L. Thermodynamic modeling of the Pd-Zr system. *Calphad* **2006**, *30*, 482–488.
7. Nishiura, T.; Yamamuro, T.; Hashimoto, D.; Morizono, Y.; Nishida, M. Martensitic transformation and phase equilibrium in near equiatomic Zr-Pd alloys. *Mater. Sci. Eng. A* **2006**, *438–440*, 852–856. [CrossRef]
8. Maeland, A.J.; Lukacevic, E.; Rush, J.J.; Santoro, A. Neutron powder diffraction and inelastic scattering study of the structures of Zr_2Pd, $Zr_2PdD_{1.70}$ and $Zr_2PdD_{1.96}$. *J. Less Common Met.* **1987**, *129*, 77–91. [CrossRef]
9. Matsuki, H.; Ibuka, H.; Saka, H. TEM observation of interfaces in a solder joint in a semiconductor device. *Sci. Technol. Adv. Mater.* **2002**, *3*, 261–270. [CrossRef]